

## Flow rule of dense granular flows down a rough incline

Tamás Borzsonyi<sup>1,2</sup> and Robert E. Ecke<sup>1</sup><sup>1</sup>Condensed Matter and Thermal Physics and Center for Nonlinear Studies, Los Alamos National Lab, NM, 87545, USA<sup>2</sup>Research Institute for Solid State Physics and Optics, POB 49, H-1525 Budapest, Hungary

(Dated: April 15, 2024)

We present experimental findings on the flow rule for granular flows on a rough inclined plane using various materials including sand and glass beads of various sizes and four types of copper particles with different shapes. We characterize the materials by measuring  $h_s$  (the thickness at which the flow subsides) as a function of the plane inclination on various surfaces. Measuring the surface velocity  $u$  of the flow as a function of flow thickness  $h$ , we find that for sand and glass beads the Pouliquen flow rule  $u = \sqrt{gh}$  ( $h = h_s$ ) provides reasonable but not perfect collapse of the  $u(h)$  curves measured for various and mean particle diameter  $d$ . Improved collapse is obtained for sand and glass beads by using a recently proposed scaling of the form  $u = \sqrt{gh} = h \tan^2 \alpha = h_s \tan^2 \alpha_1$  where  $\alpha_1$  is the angle at which the  $h_s(\alpha)$  curves diverge. Measuring the slope for ten different sizes of sand and glass beads, we find a systematic, strong increase of  $\alpha_1$  with the divergence angle  $\alpha$  of  $h_s$ . The copper materials with different shapes are not well described by either flow rule with  $u \propto h^{3/2}$ .

PACS numbers: 47.57.Gc, 45.70.-n

## I. INTRODUCTION

Granular flow on a rough inclined plane is an important system with which to learn about the basic rules of the dynamics of granular materials [1, 2, 3, 4, 5, 6, 7, 8, 9]. Despite intensive study, the fundamental features of such flows are still incompletely understood (for reviews see: [10, 11, 12]). The majority of laboratory experiments report on the flow properties in narrow channels (quasi-2D geometry) where the velocity can be measured as a function of depth by directly viewing grain motion through the sidewalls [5, 6, 7, 8, 9, 10, 13, 14, 15]. In this configuration, however, the effect of friction with the confining vertical walls is important [10, 15, 16, 17], and remains a determining force for thick flows (flow on a pile) even in wider channels [17, 18].

For thin flows in wide channels measuring the depth dependence of the flow velocity (far from the side walls) is far more difficult. To characterize the basic features of granular flows in this configuration, the surface velocity  $u$  or the depth averaged velocity  $U$  can be measured as a function of the flow thickness  $h$ . The depth averaged flow velocity  $U$ , inferred from the front velocity of the granular layer, was systematically measured by Pouliquen as a function of the flow thickness  $h$  for glass beads over a range of plane inclinations [2]. The  $U(h)$  curves measured at different values of  $\alpha$  collapsed when using the scaling law  $U = \sqrt{gh} = h \tan^2 \alpha = h_s \tan^2 \alpha_1$  (where  $h_s$  corresponds to the thickness where the flow subsides) giving rise to a general flow rule, denoted the "Pouliquen flow rule," for glass beads with various sizes and for which  $\alpha_1 \approx 0.14$  and  $0.1$ . It was subsequently reported [3] that the same scaling collapsed the  $U(h)$  curves for sand with one par-

ticular size of  $d = 0.3 \text{ mm}$ . The slope for the sand data,  $0.65$ , was considerably larger than for glass beads and  $0.77$ . This quantitative difference in the flow rule was used to explain complex dynamical phenomena, such as waves [3] or avalanche propagation [19].

It is of considerable interest to determine the robustness of the Pouliquen flow rule (PFR) for different flow conditions including particle diameter, relative surface roughness, and particle shape. A further consideration is whether the flow rule is sensitive to measuring the front velocity as compared to measuring the surface velocity. The former yields a better depth averaged velocity but is subject to saltating grains for faster flows which limited the accuracy of the measurement to about 10 % [2] and would not be applicable for general granular materials subject to a lingering instability [20]. The surface velocity measurement is characteristic of the steady flow even for general granular media and avoids the accuracy limitations imposed by saltation, but can only be related to a depth-average by some assumption of the vertical velocity profile. Neither approach is ideal, being rather complementary as opposed to one being a priori better than the other. Our work establishes the utility and robustness of using the surface velocity to determine the flow rule. If a flow rule is to be a useful measure of the state of granular flow on an incline, it should not be particularly sensitive to the details of its determination.

A recent theory by Jenkins [21] suggests a phenomenological modification of the hydrodynamic equations for dense flows. According to the theory enduring contacts between grains forced by the shearing reduce the collisional rate of dissipation while continuing to transmit force and momentum. This assumption has several consequences, one of which is a modification of the Pouliquen scaling law by the inclusion of a  $\tan^2$  correction to the  $h = h_s$  term. Repplotting the Pouliquen data, Jenkins found a better collapse of the data using his modified

Electronic address: btamas@szfki.hu

form, denoted here as the "Pouliquen-Jenkins" flow rule (PJFR). The improvement of the collapse, however, was not definitive owing to the scatter in the velocity data and in the associated determination of the  $h_s(\cdot)$ .

One of the purposes of a flow rule is to have a compact description of easily measurable quantities that represents the subtle balances of stress and strain rate in a granular material, i.e., the granular rheology. Although the vertical velocity profile in a flowing granular layer has not been obtained experimentally, let alone the experimental determination of local stresses and strain rates, a general discussion about possible flow rheologies helps set a background for presenting empirical flow rules determined from experiment. In particular, the scaling of the velocity with layer thickness can be understood by a consideration of bulk Bagnold rheology [1, 22]. In the theory of Bagnold, the shear stress varies with the shear rate  $\dot{\gamma}$  like  $\dot{\gamma} \propto \tau$ . This relationship is based on the following assumptions. The transport of the  $x$  component of momentum in the  $z$  direction occurs through collisions whose rate depends on the velocity gradient  $\dot{\gamma}$ . Similarly the momentum transfer per collision scales linearly with  $\dot{\gamma}$  leading to the quadratic dependence between stress and strain. With a linear dependence of shear stress on the vertical coordinate  $z$ , this leads to a vertical variation of the down-plane velocity of  $u(z) \propto h^{3/2} \dot{\gamma}^{1/2} ((h-z)/h)^{3/2}$ . Thus, the surface velocity  $u = u(h) \propto h^{3/2}$  so that the scaling  $u = \dot{\gamma}^{1/2} gh$  versus  $h$  (suitably corrected for inclination angle) should yield straight lines with zero intercept. Such scaling was reported for experiments [2, 23] using glass spheres and for numerical simulations of idealized spherical particles [22]. Also, deviations from this law towards a linear velocity profile were reported in experimental [23] and numerical [24] studies for thin flows. For a particular flow profile, the surface velocity  $u$  and the depth averaged velocity  $U$  are related by a constant factor. Thus, there is no a priori reason to prefer one over the other. Although the interior velocity profile far from sidewalls has not been measured to our knowledge, the scaling  $u \propto h^{3/2}$  is indirect support for the Bagnold flow rheology. The degree to which such scaling fails, therefore, would appear to call for modification of the assumptions leading to the Bagnold rheology. We will see in this paper how well the Bagnold-based rheology applies to a range of different granular materials.

In the present work we investigate the flow properties of 14 different materials by measuring the surface velocity  $u$  as a function of flow thickness  $h$ . Because of our measurement methods, the statistical uncertainty in our data is considerably less than in previous studies [2], allowing for a more detailed and quantitative evaluation of different flow rule scalings. We find that scaling the surface flow velocity by  $\dot{\gamma}^{1/2} gh$  and the flow thickness by  $h_s$  assuming the Pouliquen flow rule provides reasonable but not perfectly accurate collapse of the  $u(h)$  curves taken at various plane inclina-

tions measured in a wider range of the main control parameters of grain size, plane inclination angle, surface roughness and flow thickness compared to earlier studies [2, 3, 23]. Improved collapse is obtained for sand and glass beads using the modified Pouliquen-Jenkins scaling law  $u = \dot{\gamma}^{1/2} gh = \dot{\gamma}^{1/2} h \tan^2 \phi_s = h_s \tan^2 \phi_1$  where the factor  $\tan^2 \phi_1$  is supported by a recent theory [21]. For glass beads the straight lines of the scaled curves support the Bagnold rheology. For sand, although the data are well collapsed by the scaling, the curves are slightly concave downward suggesting high-order corrections in  $h$  beyond the simple Bagnold result. We show that the slope of the master curve for the sand/glass-bead materials (obtained for each material) strongly increases with  $\tan \phi_1$  or  $\tan \phi_r$  where  $\phi_1$  and  $\phi_r$  are the angles where  $h_s(\cdot)$  diverges and the bulk angle of repose, respectively. The similarities and differences of our experimental approach compared to other experimental measurements of flow rules [2, 23] are discussed in detail.

In contrast to the relatively simple and understandable data obtained for glass beads and for sand, the behavior of flowing copper particles is more complex and a simple Bagnold interpretation works quite poorly in describing the relationship between surface velocity and layer height. Indeed, the scaling of  $u$  with  $h$  is closer to  $u \propto h^{1/2}$  than to the Bagnold form  $u \propto h^{3/2}$ . Nevertheless, the angle correction using  $h_s(\cdot)$  (Pouliquen flow rule) or  $h_s(\cdot) = \tan^2 \phi$  (Pouliquen-Jenkins flow rule) appears to work pretty well with the latter again providing better overall data collapse.

## II. EXPERIMENT

The experimental measurements presented in this paper were performed in two different setups. The first apparatus was described in detail elsewhere [25] and consisted of a glass plate with dimensions 230 cm x 15 cm (see Fig. 1). The leftmost 40 cm of the plate served as

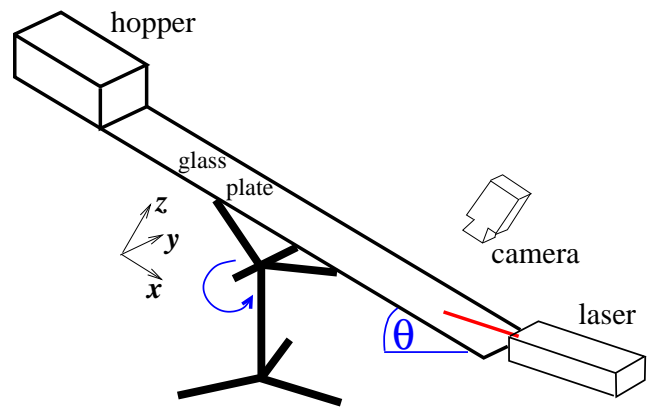


FIG. 1: (Color online) Schematic of the experimental setup used to measure the surface velocity and height. The whole system could be rotated (together with laser and camera) to set an arbitrary inclination angle  $\theta$ .

the bottom of the hopper. The surface of the remaining part (190 cm) of the glass plate was typically covered with sandpaper that was glued to the surface and had a roughness of  $R = 0.19$  mm (grit 80) which provided an extremely durable uniform roughness to the plate. Other values of plate roughness were studied using different grit sandpaper (and a few measurements with 0.4 mm sand glued to the glass plate) to explore the systematic dependence of our results on relative roughness compared to grain size. The plate together with the hopper could be tilted, enabling us to set an arbitrary inclination angle. The flow was characterized by measuring the surface velocity  $u$  as a function of the thickness  $h$  in the stationary dense flow regime at a location  $x_0 = 155$  cm below the hopper gate, sufficiently far downstream to have established a steady state [25]. This first apparatus could be tilted back and forth to recharge the hopper, facilitating the accumulation of the large amounts of data reported here. Because the system was closed in a cylindrical tube, precise measurements of  $h_s(\phi)$  were difficult and were performed in a second apparatus.

The second apparatus used to measure  $h_s(\phi)$  consisted of a wider plate having dimensions 227 cm  $\times$  40 cm and was covered with the same sandpaper used to cover the surface of the flow channel. The system was not connected from the top. This wider, non-enclosed channel allowed for very precise measurements of the layer height in a rapid manner. The procedure was to throw the grains onto the plane and allow a uniform layer thickness to form by letting the flow subside. The granular material was swept from a 2 m long area and its volume was measured accurately, yielding a very precise and repeatable measurement of the mean layer thickness  $h_s(\phi)$ . This method averages out the spatial variations in  $h_s$ , the amplitude of which was also estimated by measuring the displacement of a projected laser sheet. At lower  $\phi$ , the height variations were typically less than 5% of  $h_s$ , but became larger at higher plane inclinations where  $h_s$  became less than  $5d$ . Because the majority of the data on the flow properties were measured at plane inclinations corresponding to these relatively lower values of  $h_s$ , it is important to get an accurate measure of  $h_s$ . The repeatability of the measurement also depended on the plane inclination, but in this case relative variations decreased with increasing  $\phi$ . The data points fell onto the same curve within an error of 5% for  $\tan \theta = \tan \theta_c > 1.1$ . When approaching  $\theta_c$  the measurements became less accurate with the rapid increase of  $h_s$  leading to a 12% uncertainty of the data points for  $\tan \theta = \tan \theta_c < 1.1$ .

Uncertainties arising from slightly nonuniform thickness near the walls were also estimated. We observed a boundary layer  $W$  where the layer thickness was slightly larger than elsewhere. The width of the boundary layer was  $W < 1$  cm for  $\tan \theta = \tan \theta_c > 1.1$  and somewhat larger  $W < 5$  cm for smaller  $\phi$ . The effect of the boundary layer results in a slight overestimation of  $h_s$  corresponding to about 2% for  $\tan \theta = \tan \theta_c > 1.1$  and 5% for smaller  $\phi$ . To reduce the effect of the boundary layer we

removed part of the excess material near the boundary, and we estimate that the normally measured value of  $h_s$  is overestimated by less than 1% owing to the effect of the lateral boundaries.

A possible concern regarding using one apparatus to measure  $h_s(\phi)$  and another to measure  $u$  and  $h$  in the flowing state is that the lateral boundary effects might be different, leading to possible discrepancies in the measurements. To that end we measured the flow profile in the narrow channel, as presented below, and found that the flow was uniform over the central 80% of the narrow channel. Because our measurements of  $u$  and  $h$  were taken in the center of the narrow channel, we conclude that no significant differences arise from using different channels for the static and dynamics measurements, respectively. Further, because of the limitations of each system, the amount of data we obtained would not have been feasible using one or the other of our experimental setups.

Four types of granular materials were used. The first set consisted of sand particles from the same origin but sorted into four different sizes. For example, the first sample was obtained by sifting the sand with 100 and 300  $\mu$ m sieves. We designate this distribution as having a mean of  $d = 0.2$  mm and a standard deviation of 0.05 mm. According to this notation the four sets of sand correspond to sizes  $d = 0.2 \pm 0.05$  mm,  $d = 0.4 \pm 0.05$  mm,  $d = 0.6 \pm 0.05$  mm and  $d = 0.85 \pm 0.08$  mm while the mean particle density was  $\rho_{\text{sand}} = 2.6$  g/cm<sup>3</sup>. The fifth sample of sand originated from the Kelso dunes and was well sorted with a size distribution of  $d = 0.2 \pm 0.05$  mm. This sand is peculiar in that it emits sound when sheared. The Kelso dune is known to be an example of "booming sand dunes" [26]. We also used commercial

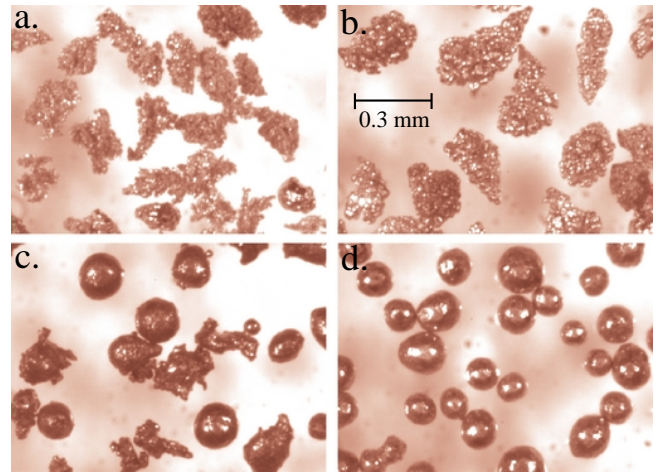


FIG. 2: (Color online) Microscopic images of the copper particles with  $d = 160 \pm 50$   $\mu$ m and with packing fractions: a) 0.25, b) 0.33, c) 0.5 and d) 0.63.

glass beads (Cathapote) with sizes  $d = 0.18 \pm 0.05$  mm,  $d = 0.36 \pm 0.05$  mm,  $d = 0.51 \pm 0.05$  mm and  $d = 0.72 \pm 0.08$  mm and mean particle density of  $\rho_{\text{glass}} = 2.4$  g/cm<sup>3</sup>.



One sample of the  $d = 0.51 - 0.05$  mm glass beads was carefully washed. For that sample, we observed a slight change in the flow properties as well as in the value of  $h_s$  compared to an unwashed sample with the same  $d$  and, thus, we report these data as an additional case. The last type of material consisted of copper particles with a mean size of  $d = 0.16 - 0.03$  mm but with different shapes. The shape anisotropy of the four different samples of copper particles is characterized by the volume fraction (the ratio of the volume occupied by the particles and the total volume) of the material at rest, with values 0.63, 0.5, 0.33, 0.25 and particle densities 8.7, 8.2, 7.6, 7.1 g/cm<sup>3</sup>, respectively. The variation in  $\eta$  represents the strong change in the shape from spherical particles to very dendritic shapes with decreasing particle densities for the more dendritic shapes as well. Images of copper particles are shown in Figs. 2(a)-2(d) where the strong variation in particle shapes is clearly seen.

The surface flow velocity  $u$  was determined by analyzing high speed (8000 frames per second) video recordings. Individual particles make streaks in a space-time plot of intensity along one line of camera pixels aligned with the mean flow direction. An example of such a space-time image is shown in Fig. 3(b) where the length of the line in the camera is  $L = 3.68$  cm and the total time is  $T = 0.080$  s. The streaks are generally oriented at some

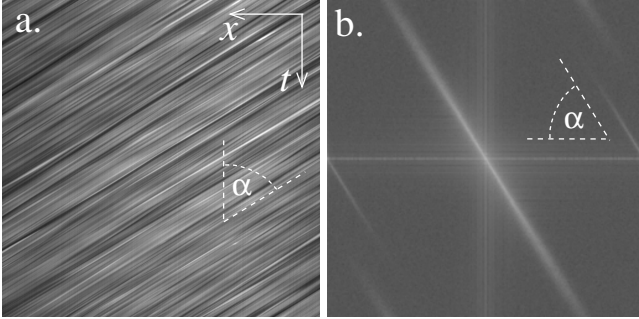


FIG. 3: a) Space time plot showing particle streaks along a line oriented with the flow direction for  $\theta = 36.1^\circ$  and  $H = 2$  cm. Dimensions of the image are 3.68 cm and 0.08 s. b) Two dimensional FFT in frequency/wave-number space of the image in a) which gives an accurate measure of the mean flow velocity as indicated by the solid line. The angle  $\alpha$  is designated in each image.

angle  $\alpha$  in the image. Performing a fast Fourier transform (FFT) produces a line perpendicular to the streaks, see Fig. 3, which gives a measure of the mean surface velocity  $u = (L/T) \tan \alpha$ . The thickness  $h$  of the flow was monitored by the translation of a laser spot that was projected onto the surface of the plane at an angle of  $\theta = 20^\circ$  in the  $xz$  plane (see Fig. 1). Other details regarding the measurement techniques can be found in [25].

### III. RESULTS AND DISCUSSION

The two measurements that determine the flow rule are the height of the layer when the flow stops  $h_s(\theta)$  and the dependence of the surface velocity on the layer height  $h$ . We first consider  $h_s(\theta)$  for glass beads, sand and copper. We then present measurements of  $u$  as a function of  $h$  for sand and glass beads and the application of the flow rules of PFR and PJFR. Finally, we consider velocity data and flow rules for the copper material.

#### A. Determination of $h_s(\theta)$

As seen in Figs. 4(a)-4(c),  $h_s$  increases rapidly with decreasing  $\theta$  and diverges at  $\theta_1$ . The solid lines in Fig. 4 are

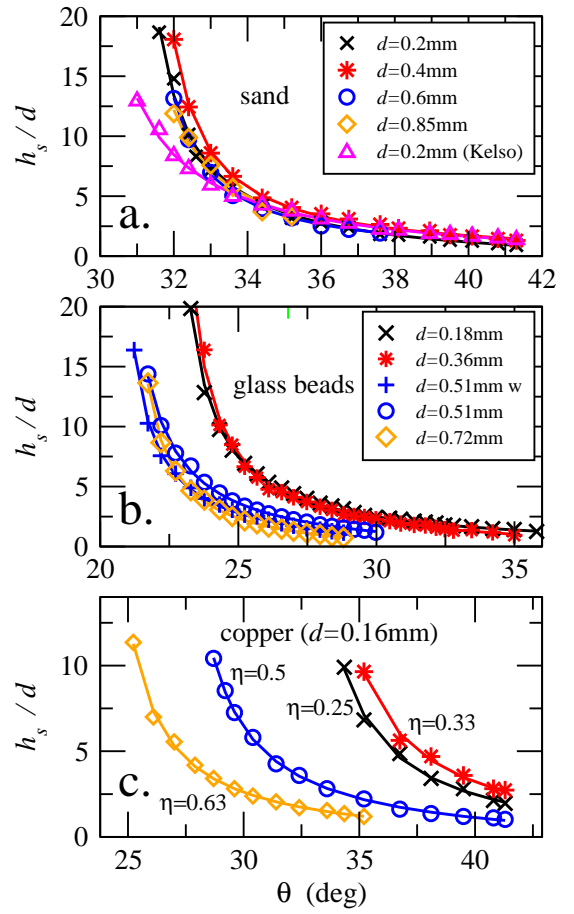


FIG. 4: (Color online) The thickness  $h_s$  at which the flow subsides normalized by the grain diameter  $d$  as a function of the plane inclination angle  $\theta$  for a) sand and b) glass beads of various sizes and c) copper particles of various shapes (as indicated by the static volume fraction  $\eta$ ). The grain diameter  $d$  is indicated and  $w$  designates the case of washed glass beads. The continuous lines are best fits according to the formula  $h_s/d = B (\tan^2 \theta - \tan^2 \theta_1) = (\tan \theta - \tan \theta_1)$ . The resulting values of  $\theta_1$  are indicated for each material in Table I.

best fits to the formula  $h_s/d = A (\tan^2 \theta - \tan^2 \theta_1) = (\tan$

$\tan \theta_1$ ), a simple function which diverges at  $\theta_1$  and goes to zero at  $\theta_2$  [2, 3, 10, 27]. The resulting values for the fitting parameters  $A$ ,  $\theta_1$ , and  $\theta_2$  are indicated for each material in Table I. The bulk angle of repose  $\theta_r$  was also measured for several materials by measuring the dynamics of a three dimensional sandpile under constant flux conditions. As material was added at a very small but uniform rate to the top of the pile, avalanches formed and propagated downward intermittently. The distribution of the angle, observed directly after the avalanche stopped, was measured for hundreds of avalanches. The mean of this distribution was taken to be  $\theta_r$ , the bulk angle of repose. The value of  $\theta_r$  is very close to  $\theta_1$  as indicated in Table I.

The  $h_s(d)$  curves are very similar for all four sand samples originating from the same source [see Fig. 4(a)]. The fifth curve corresponding to the Kelso sand showed deviations from the other data at lower values of  $d$ , yielding a somewhat smaller value for  $\theta_1$ . This difference is attributable to the more rounded shape for the Kelso sand as revealed in microscope images. The  $h_s(d)$  curves for glass beads, however, formed two groups. Microscope images revealed that the two samples with smaller  $d$  contained a larger amount of non-spherical particles than the two sets with larger  $d$ .

sand					
d [mm]	0.2	0.4	0.6	0.85	0.2 (K)
$\theta_r$	30.6°	30.5°	—	—	—
$\theta_1$	30.6°	30.8°	30.6°	30.5°	28.9°
$\theta_2$	46.4°	51.3°	47.7°	47.7°	52.4°
A	1.05	0.83	0.9	0.92	0.92
glass beads					
d [mm]	0.18	0.36	0.51	0.51 (w)	0.72
$\theta_r$	—	—	—	20.9	—
$\theta_1$	22.2°	22.3°	20.3°	20.3°	20.8°
$\theta_2$	60.9°	47.7°	43.5°	42.9°	34.2°
A	0.33	0.69	0.73	0.58	0.95
copper particles					
$\eta$	0.25	0.33	0.5	0.63	
$\theta_r$	33.8°	33.5°	27.9°	23.9°	
$\theta_1$	32.2°	32.7°	26.7°	23.4°	
$\theta_2$	60.9°	64.5°	58.0°	50.2°	
A	0.49	0.46	0.46	0.59	

TABLE I: The values of  $\theta_r$ ,  $\theta_1$ ,  $\theta_2$  and  $A$  for sand and glass beads of size  $d$  and copper particles with  $d = 0.16$  mm and volume fractions  $\eta$ . K stands for the Kelso sand, and w denotes the washed glass beads.

The difference in shape may explain the slightly larger values of  $\theta_1$  and  $h_s=d$  for the two samples with smaller  $d$ . The case of the 0.51 mm glass beads is also interesting in that washing the material with tap water resulted in a slightly smaller value of  $h_s$ , which implies slightly reduced friction either with respect to the rough surface or between individual grains. The reduction could have been caused by the elimination of non-spherical dust particles owing to washing the sample. The four samples of copper

are nice examples of the effect of particle shape. A systematic increase of  $\theta_1$  and  $\theta_r$  detected by changing shape anisotropy in the order of spherical beads ( $\eta = 0.63$ ), particles with irregular but rounded shapes ( $\eta = 0.5$ ) and the two sets of particles with very anisotropic dendritic shapes ( $\eta = 0.25$  and  $\eta = 0.33$ ).

The influence of the boundary conditions can have a profound effect on the conditions of the granular flow. The usual no-slip boundary condition appropriate for a fluid is probably never completely satisfied for a granular flow and certainly depends on surface roughness. Further, the role of the surface in damping energy is only recently beginning to attract attention [28] and has not been considered in the context of granular flows on an incline. Thus, it is important to evaluate the dependence of our results on surface roughness and, in principle, on surface restitution coefficient. Although we do not consider the latter here, the systematic of a flow rule comparison may depend on the damping properties of the surface which may help explain differences between flow on a soft felt surface, on a glass plate with glued on hard particles, or a hard surface covered with sandpaper.

To study the dependence of our results on surface roughness, we measured the dependence of  $h_s=d$  on plane roughness  $R$ , shown in Figs. 5(a) and 5(b) for sand with  $d = 0.4$  mm and glass beads with  $d = 0.36$  mm on four different sandpapers with nominal roughness of  $R = 0.12$  mm,  $R = 0.19$  mm,  $R = 0.43$  mm and  $R = 0.69$  mm (grits 120, 80, 40 and 24 respectively). For sand  $h_s=d$  was also determined on a surface prepared by gluing one layer of the same grains onto the plate. For both sand and glass beads, Figs. 5(a) and 5(b), a slight increase of  $h_s=d$  is observed with increasing plane roughness. For the case of sand with  $d = 0.4$  mm the curve measured on the surface prepared by gluing the same grains was the most similar to the curves taken on sandpaper with  $R = 0.12$  mm or  $R = 0.19$  mm, i.e., the surface friction for sandpaper is somewhat larger than when the surface is covered with sand glued to the surface.

We determine the relative effect of surface roughness on the determination of  $h_s$  by comparing data for sand and glass beads for different values of  $d$  and  $R$ . The value of  $h_s=d$  increases as a function of  $R=d$  as shown for three values of  $\tan \theta = \tan \theta_r$  in Fig. 5(c). At plane inclinations close to the bulk angle of repose  $\theta_r$ , the curve seems to saturate [see the curve taken at  $\tan \theta = \tan \theta_r = 1.1$  in Fig. 5(c)] but for larger plane inclinations, i.e., for thinner layers, a slight increase of  $h_s=d$  is observed over the measured range of  $R=d$ . The increasing tendency of  $h_s=d$  indicates that the effective friction near a rough surface increases slightly with increasing plane roughness. Near the rigid surface the particles have less freedom to rearrange so that in order to shear the medium has to dilate more [29] yielding a larger effective friction, compared to the case of the bulk material. The growing value of  $h_s=d$  matches the overall tendency of the data reported in [10] using monodisperse glass beads on surfaces prepared by gluing one layer of glass beads on a plate. We did

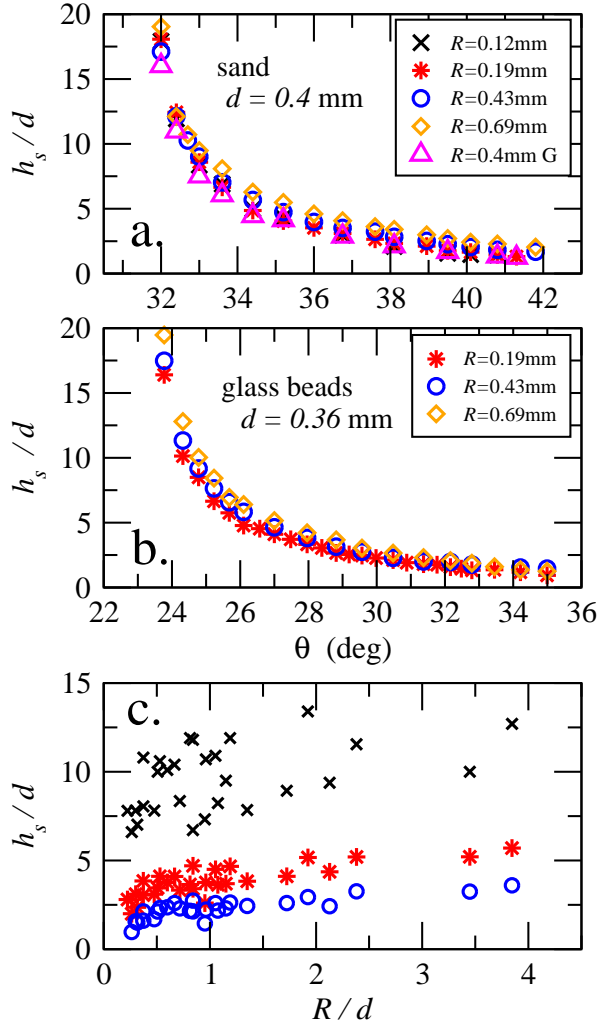


FIG. 5: (Color online)  $h_s$  vs.  $\theta$  for a) sand with  $d = 0.4$  mm and b) glass beads with  $d = 0.36$  mm for various values of surface roughness: surface covered by sandpaper with  $R = 0.12$  mm (x),  $R = 0.19$  mm (?),  $R = 0.43$  mm (o) and  $R = 0.69$  mm (◇), surface covered by one layer of  $d = 0.4$  mm sand particles (△). c)  $h_s/d$  as a function of  $R/d$  for  $\tan \theta = \tan \theta_c = 1.1$  (x);  $1.25$  (?); and  $1.4$  (o) for sand and glass beads.

not, however, find any significant height maximum corresponding to a particular plane roughness reported in [10, 30]. Note that a stronger difference in  $h_s/d$  was detected when the values measured on a solid rough surface (similar to our case) and on velvet cloth were compared [10]. As discussed above, this may be more a result of surface damping than surface roughness.

The homogeneous dense-flow regime existed for moderate plane inclinations where  $\tan \theta = \tan \theta_1$  was in the range  $1.1 - 1.45$ . According to our measurements [25], the density of the flow in this regime was decreased slightly with increasing  $\theta$  but was always larger than  $0.8 \rho_s$  where  $\rho_s$  is the close packed static density of the material, in accordance with other experimental data [2, 3] and with numerical simulations [22, 24, 31].

## B. Flow rule for glass beads and sand

We next present measurements of flow velocity obtained using the space-time technique described above. To demonstrate that sidewall boundaries do not affect the velocity near the channel center, we consider the transverse velocity profiles shown in Fig. 6 for a hopper opening of  $H = 2$  cm for several values of  $\theta$ . The data show that friction with the smooth sidewalls is much less

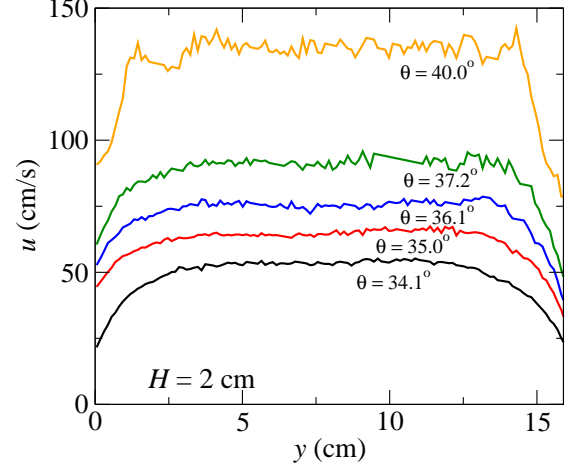


FIG. 6: (Color online) Transverse velocity profiles of the flow for sand with  $d = 0.4$  mm at a hopper opening of  $H = 2$  cm.

important than friction with the rough bottom plate so that the sidewalls only produce a lateral boundary layer at the edge of the channel with a characteristic thickness of 2–3 cm. Over the remaining 80% of the channel width,  $u$  is very constant. For determination of the flow rule, the velocity  $u$  and thickness  $h$  were measured at the channel center.

We now consider  $u$  as a function of  $h$  for sand and glass beads, presented in a variety of forms to test both PFR [2] and PJFR [21]. In Figs. 7(a) and 7(b), we show  $u$  as a function of the flow thickness  $h$  for sand with  $d = 0.4$  mm and glass beads with  $d = 0.36$  mm. In Figs. 7(c) and 7(d), the same data are presented in dimensionless form according to the flow rule  $u = \frac{\rho_s g h}{\mu} h = h_s$  suggested by Pouliquen [2]. For comparison, we include the curves measured by Pouliquen for glass beads with  $d = 0.5$  mm and sand with  $d = 0.8$  mm [3], correcting for the difference between depth averaged velocity  $U$  and surface velocity  $u$  that assumes a Bagnold velocity profile for which  $u = 1.67U$ .

Our data cover a wider range of  $u$  and  $h$  than previously measured, partly because of the smaller grain size, but also owing to the measurement technique. Namely, measuring the surface velocity in the stationary regime was much more straightforward for us than detecting the velocity of the front and thereby determining  $U$ . For the detection of the front velocity the difficulty was that in contrast to the simple monotonic increase of the height at the flow front (reported in [2]), in some cases and partic-

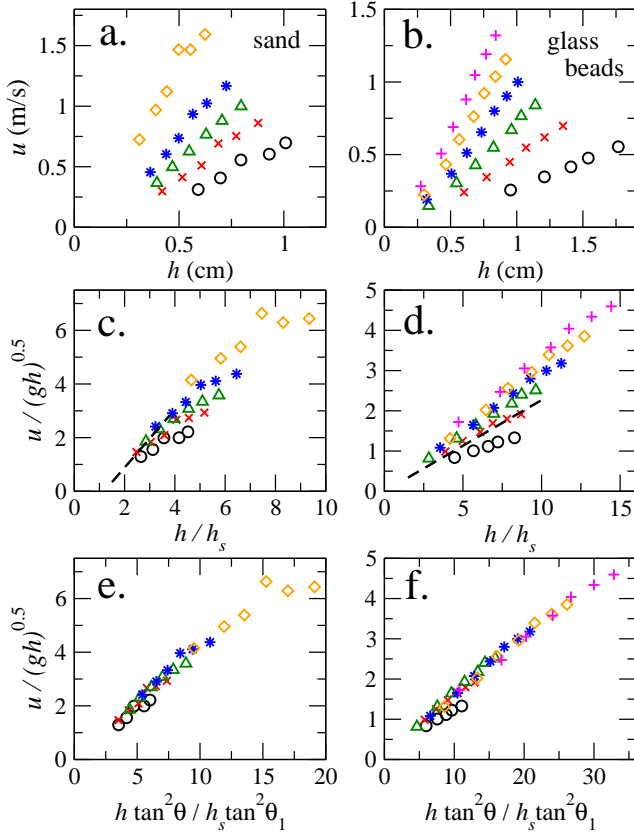


FIG. 7: (Color online) The flow velocity  $u$  as a function of  $h$  for a) sand with  $d = 0.4$  mm and b) glass beads of  $d = 0.36$  mm. Corresponding values of  $\theta$  for a) sand 34:1 ( $\circ$ ), 35:0 ( $\times$ ), 36:1 ( $\square$ ), 37:2 ( $\triangleright$ ), 40:0 ( $\circ$ ); b) for glass beads 25:6 ( $\triangleright$ ), 26:8 ( $\times$ ), 28:0 ( $\square$ ), 29:4 ( $\triangleright$ ), 30:7 ( $\circ$ ), 32:0 ( $+$ ).  $u = \sqrt{gh}$  vs  $h = h_s$  for c) sand and d) glass beads.  $u = \sqrt{gh}$  for e) sand and f) glass beads vs.  $h \tan^2 \theta / h_s \tan^2 \theta_1$ .

ularly for anisotropic grains we observed a larger height in the vicinity of the front. In other cases, typically for larger (spherical) grains, the front was less defined with some grains rolling ahead of the front, i.e., saltating.

The collapse of the data curves for sand and glass beads in Figs. 7(c) and 7(d) is not perfect. In these dimensionless units higher plane inclinations still result in somewhat faster flow. We therefore consider the modified PJFR scaling [21] that includes a  $\tan^2$  correction to the  $h = h_s$  term. In Figs. 7(e) and 7(f), we plot our data in terms of this modified scaling form, namely,  $u = \sqrt{gh}$  versus  $h \tan^2 \theta / h_s \tan^2 \theta_1$ . The PJFR produces improved scaling relative to PFR as demonstrated in Figs. 7(c) and 7(d). Another consequence of the theory is a prediction for the density decrease with increasing  $\theta$  as  $\rho_s = 1/B \tan^2 \theta$  (where  $\rho_s$  stands for the close packed static density). Our data for the mean density, reported elsewhere [25], are well fit by the theoretical form with a value  $B = 0.52$ .

We next extend our comparison of flow rules to the whole set of sand and glass beads used in this study.

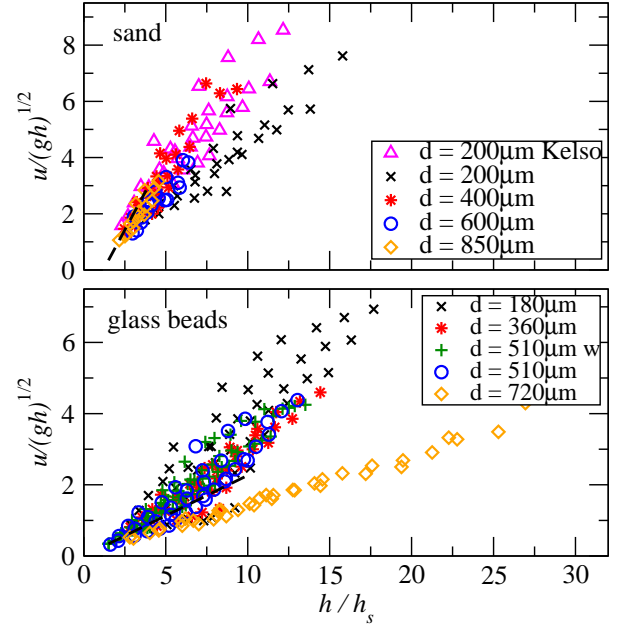


FIG. 8: (Color online) Dimensionless flow velocity  $u = \sqrt{gh}$  vs  $h = h_s$  for sand and glass beads as a test of PFR. The grain diameter  $d$  is indicated and  $w$  designates the case of washed glass beads. The dashed lines correspond to the velocity data taken for glass beads with  $d = 0.5$  mm and sand with  $d = 0.8$  mm from [3].

The data taken for these materials were scaled in the same manner as in the case of sand with  $d = 0.4$  mm and glass beads with  $d = 0.36$  mm as presented in Figs. 7(c) and 7(d), i.e., using PFR. In Fig. 8, we plot  $u = \sqrt{gh}$  as a function of  $h = h_s$  for sand and glass beads with a variety of sizes. The scatter of the data is a sign of an imperfect collapse for each material. For comparison the flow rule measured by Pouliquen for sand and glass beads is included (dashed lines) and agrees with the data scatter with our measurements. Plotting  $u = \sqrt{gh}$  as a function of  $h \tan^2 \theta / h_s \tan^2 \theta_1$  for sand and glass beads yields an improved collapse, see Figs. 8 and 9.

There are two things to notice about the curves in Figs. 8 and 9, focusing more on the latter. First, there is the linearity of the lines for different  $d$ . The glass bead data form quite nice straight lines in support of a simple Bagnold rheology with  $u \propto h^{3/2}$ . There is some remnant dependence on  $d$  discussed below. The sand data are quite well collapsed and have a weaker variation on the grain size. The curves are, however, not straight lines but are slightly concave downward. This deviation from linearity suggests a modification of the Bagnold rheology is needed but the basic form captures them in details of the scaling. Second, the nonzero offset observed for sand for the case of the Pouliquen flow rule (Fig. 8) becomes approximately zero for the modified scaling relationship (see Fig. 9). This leads to a simpler quantitative comparison of these materials as the curves are characterized by a single parameter.



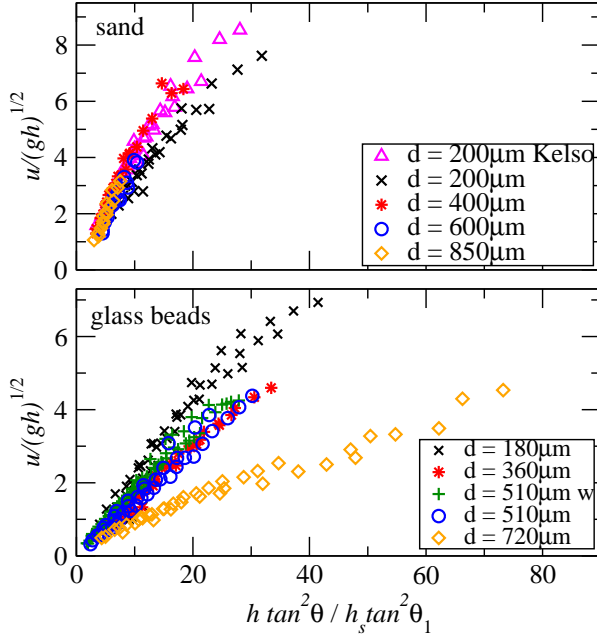


FIG. 9: (Color online) Dimensionless flow velocity  $u = \frac{p}{\rho gh}$  vs  $h \tan^2 \theta = h_s \tan^2 \theta_1$  for sand and glass beads as a test of PJFR.

We now consider some of the details of the data from the perspective of the particle size  $d$ . Comparing the curves measured for various materials in Fig. 9, we find curves with similar slopes for sand of different sizes. Similarly, for glass beads the slopes of the curves determined using PJFR and for samples of various  $d$  do not differ much except for the material with  $d = 0.72$  mm where is considerably smaller. This difference cannot be quantitatively explained, but the case of the  $d = 0.72$  mm glass beads could be special because the  $R=d$  ratio is very small (0.26) in this case. For spherical beads there is a threshold value of  $R=d$  below which the beads simply roll down the plane. As we approach this threshold by decreasing  $R=d$  the value of  $h_s=d$  drops rapidly. There is a stronger decrease of  $h_s=d$ , presumably resulting from the rolling effect of spherical glass beads, for spherical  $d = 0.72$  mm glass beads than for irregular  $d = 0.85$  mm sand particles as a function of decreasing  $R=d$ , obtained by varying the sandpaper roughness of  $R = 0.69$  mm,  $0.43$  mm and  $0.19$  mm. Using sandpaper with  $R = 0.12$  mm the  $d = 0.72$  mm beads already rolled down the plane. The low value of  $h_s=d$  could explain the low value of  $\beta$  measured for the glass beads of  $d = 0.72$  mm on sandpaper with  $R = 0.19$  mm. Generally, the collapse suggests that the modified scaling theory describes the data quite well provided the roughness ratio is larger than  $R=d > 0.3$  for glass beads and  $R=d > 0.2$  for sand.

If the flow rule provided perfect collapse of the data, there would be no residual dependence of the PJFR slope on  $d$ . This appears to be the case for the sand flows where  $\beta = 0.37$  independent of  $d$  as illustrated in Fig.

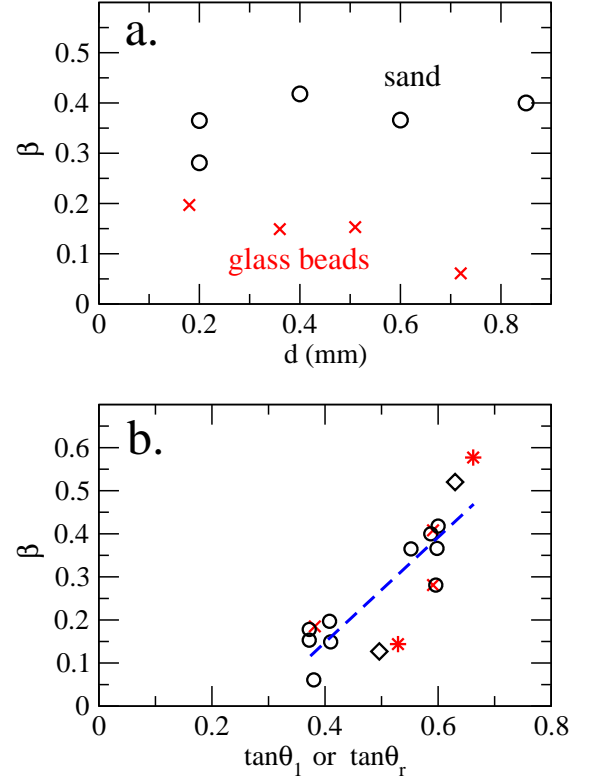


FIG. 10: (Color online) The PJFR slope  $\beta$  vs a) grain size  $d$  and b)  $\tan \theta_r$  (x) or  $\tan \theta_1$  (o) for sand and glass bead samples. The dashed line corresponds to a linear fit  $\beta = 1.22 \tan \theta_1 - 0.34$ . Slopes for copper particles (x and o) with  $\beta = 0.33$  and  $\beta = 0.50$  are included for comparison.

10 (a). On the other hand, the values of  $\beta$  for glass beads show a systematic decrease with increasing  $d$ . It is interesting that sand with its somewhat anisotropic grains is less sensitive to size variation than the more idealized glass spheres. Again the rolling effect may play an important role here.

We now consider the behavior of the sand/glass-bead materials by plotting the slope of the modified flow rule  $u = \frac{p}{\rho gh} = \frac{h \tan \theta}{h_s \tan^2 \theta_1}$  as a function of  $\tan \theta_r$  or  $\tan \theta_1$ , see Fig. 10 (b). A significant increase in  $\beta$  is observed with increasing  $\tan \theta_r$  or  $\tan \theta_1$ . In a certain sense, these angles measure the degree of frictional interactions of the grains. This finding is in general agreement with earlier more limited data [2, 3] and gives a general characterization of the materials. Although we do not have enough data to unambiguously determine a functional dependence of  $\beta$  on  $\tan \theta_1$  (or  $\tan \theta_r$ ), a linear fit to the data yields the relationship  $\beta = 1.22 \tan \theta_1 - 0.34$ .

### C. Flow rule for copper particles

The application of the flow rule scaling to the copper materials is an interesting extension beyond those materials measured previously [2, 3]. In particular, the copper



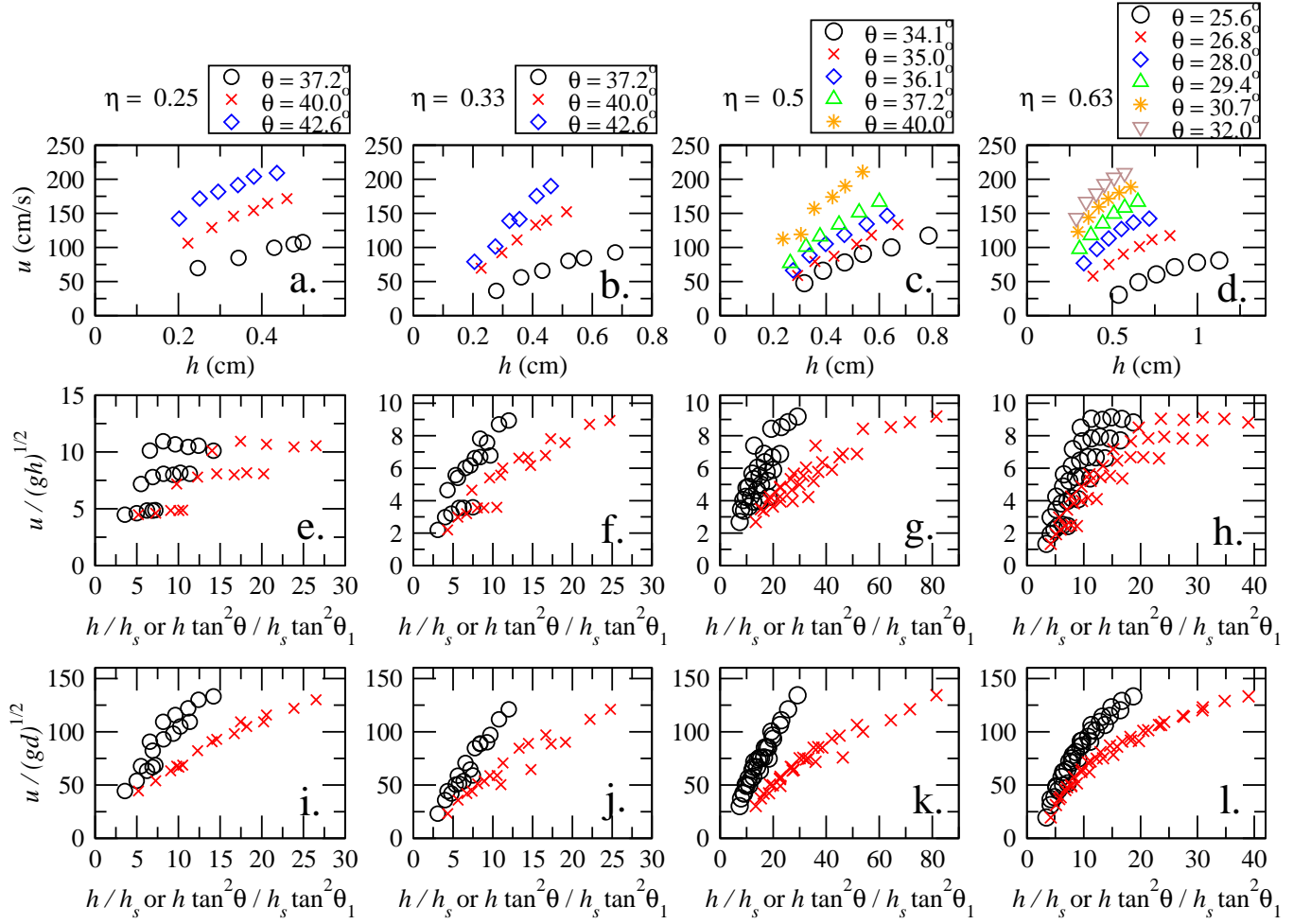


FIG. 11: (Color online) The flow velocity  $u$  as a function of  $h$  for the four set of copper particles with a)  $\eta = 0.25$ , b)  $\eta = 0.33$ , c)  $\eta = 0.5$  and d)  $\eta = 0.63$ . e-h)  $u = \sqrt{gh}$  vs  $h = h_s$  ( ) and  $h \tan^2 \theta = h_s \tan^2 \theta_1$  (x) for same  $\eta$ . i-l)  $u = \sqrt{gd}$  vs  $h = h_s$  ( ) and  $h \tan^2 \theta = h_s \tan^2 \theta_1$  (x) for same  $\eta$ , i-l).

grains are metallic and thus not affected by static charging. Further, the grains may oxidize producing different frictional contacts than for the more inert sand and glass materials. Finally, the very unusual shape anisotropy adds an additional level of complexity to the scaling problem beyond the unknown differences in shape between the sand and glass beads. We proceed in the same way for the different copper grains as with the sand/glass-bead materials in that first we show the raw data for  $u$  as a function of  $h$  in Figs. 11(a) and 11(d). The data vary smoothly with  $h$  for different values of  $\theta$ . Applying PFR or PJFR scaling as shown in Figs. 11(e)-11(h) demonstrates that either scaling does not work for the copper materials and is especially poor for the spherical copper grains with  $\eta = 0.63$ . The apparent origin of this poor collapse seems to be the assumed  $h^{3/2}$  scaling implied by a Bagnold vertical velocity profile. If instead of dividing by  $\sqrt{gh}$ , one simply plots  $u = \sqrt{gd}$  versus  $h = h_s$  or the modified form  $h \tan^2 \theta = h_s \tan^2 \theta_1$ , the curves are now approximately collapsed, see Figs. 11(i)-11(l).

In understanding this unexpected result, we first consider the spherical copper particles with  $\eta = 0.63$  for which the comparison with the sand and glass beads might be thought to be most similar. The first thing to note is that there is a distinct concave downward curvature to the raw  $u$  versus  $h$  curves in Fig. 11(d) when compared to the case of sand or glass beads. Also, the character of the scaled curves is strongly non-linear for the case of copper with  $\eta = 0.63$  and  $\eta = 0.5$  (Figs. 11(g) and 11(h)). Although we do not have a quantitative explanation for the behavior of the copper particle rheology, we note some ideas worth exploring. One issue of possible relevance is that the coefficient of restitution of soft metal particles, i.e., brass, copper, decreases with increasing velocity [32, 33] (the restitution coefficient for brass, which is harder than copper, decreases by about 8% over the range of velocities in the present experiment - 0-2.5 m/s) whereas the harder glass-bead/sand materials have a larger, velocity independent restitution coefficient. A velocity dependent (decreasing) restitution coefficient

would lead to higher dissipation at larger velocities, but this effect has not been quantitatively studied. A recent study on soft particles with constant restitution coefficient [34] suggests that the presence of long-lived contacts leads to a modified rheology with a new term (similar to a Newtonian fluid), i.e.,  $\dot{\gamma}_{xz} = A\dot{\gamma}^2 + B\dot{\gamma}$ . Such a relationship would lead to a faster growth of  $u$  with increasing  $h$  than  $u \propto h^{3/2}$ , a result that would lead to worse agreement for our copper data than did the Bagnold scaling. Part of the issue here is the indirect measure of the bulk rheology provided by comparing the dependence of  $u$  on  $h$ .

Another possible issue is the nature of the boundary condition for copper particles on the sandpaper surface. Unlike a fluid, a granular material can have a finite slip velocity at the surface. This finite velocity would complicate the scaling procedure and perhaps lead to spurious conclusions. Copper particles move somewhat faster for a given thickness  $h$  owing to their smaller size and thus may develop a larger slip velocity. For example, the copper particles have maximum velocities of order 2.2 m/s compared to 1.3–1.5 m/s for sand or glass beads over the same range of angle-corrected  $h$ .

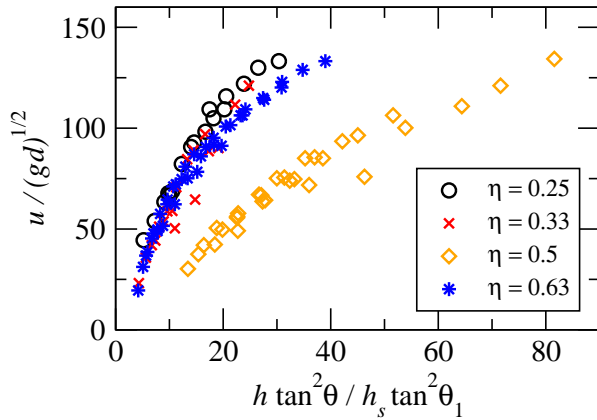


FIG. 12: (Color online) The dimensionless flow velocity  $u/(gd)^{1/2}$  as a function of the modified dimensionless flow thickness  $h \tan^2 \theta = h_s \tan^2 \theta_1$  for the four set of copper particles with  $\eta = 0.25$ ,  $\eta = 0.33$ ,  $\eta = 0.5$  and  $\eta = 0.63$ .

The other copper particles present a more complex situation. First, we plot the  $u/(gd)^{1/2}$  versus the different angle-corrected scalings in Fig. 12. The data with  $\eta = 0.25$ ,  $0.33$ , and  $0.63$  collapse rather well but the curve with  $\eta = 0.5$  has a quite different slope, about half of the other curves. The difference in slope does not come from higher velocity but rather from larger  $h$  relative to  $h_s$ . In other words larger  $h = h_s$  was needed for the realization of the stationary flow regime, which results from a relatively larger dynamic friction coefficient, the source of which may be surface oxidation of the copper particles. This results in a lower value for  $\eta$ . This set of copper is also particular in that it is the only copper sample emitting strong sound during shearing, similar to but much stronger than the Kelco sand.

Although all of the copper particle data are collapsed better by not scaling  $u$  by  $(gd)^{1/2}$ , P JFR is not so bad for the  $\eta = 0.33$  and  $\eta = 0.50$  copper particles. Extracting a slope for those values of  $\eta$  yields curves that are consistent with the sand/glass-bead scaling as a function of  $\tan \theta_1$ , see Fig. 10. Thus, even though the copper particles are quite different, they still seem to show the same qualitative dependence on  $\tan \theta_1$  as the glass-bead/sand particles.

#### IV. CONCLUSIONS

The most important findings of this work can be summarized as follows. The surface velocity  $u$  as a function of flow thickness  $h$  of a granular flow on a rough inclined plane was measured for fourteen different materials in the dense, stationary flow regime. All configurations were characterized by measuring the value of  $h_s$  (the thickness of the layer remaining on the plane after the flow subsided) as a function of the plane inclination  $\theta$ . The value of  $h_s = d$  for sand and glass beads increased slightly with increasing ratio of plane roughness and grain diameter  $R = d/m$  measured for four different values of  $R$ . The  $u(h)$  curves for sand and glass beads measured at various  $\theta$  did not perfectly collapse using the scaling law  $u = \sqrt{gh} h = h_s$  proposed by Pouliquen [2]. An improved collapse was obtained using P JFR  $u = \sqrt{gh} = \sqrt{g h \tan^2 \theta} = h_s \tan^2 \theta_1$  where the factor  $\tan^2 \theta_1$  was suggested by a recent theory by Jenkins [21]. For the sand/glass-bead materials, the P JFR slope increases strongly with  $\tan \theta_1$  yielding a quantitative description of various materials, thereby extending our tools for a better characterization and prediction of complex dynamical phenomena, such as waves [3] or avalanche propagation [19].

Our results demonstrate that when the surface velocity is used to determine the flow rule, the P JFR scaling is superior to the earlier PFR approach. For the original data set of Pouliquen [2], it is hard to determine which scaling form is better. Two possibilities are suggested. First, the uncertainty (mainly in  $h_s$ ) in the original measurements does not allow a definitive comparison. Second, measuring the depth averaged velocity at the front is substantially different from measuring the surface velocity. If the latter is correct then something unexpected is happening in the layer because Bagnold scaling (or any monotonic vertical velocity profile starting from zero velocity, for that matter) implies that the ratio of surface velocity to depth averaged velocity is a constant, and a constant factor would not change the flow rule. Although we cannot definitively rule out some strange behavior, the superiority of P JFR, the elimination of the need for an offset  $u_0$ , and the consistency of these results with Bagnold scaling suggests that the apparent discrepancy between our results and former scaling analysis [2] results from larger uncertainty in the previous measurements.

For copper grains of different shapes, neither the

Pouliquen form nor the Jenkins modified scaling works well in collapsing data taken for a variety of values of  $\phi$ . Although the angle correction works decently, the normalization of  $u$  by  $\sqrt{g h}$  produces poorer scaling. This suggests that for the copper particles, a Bagnold form for the vertical velocity profile does not hold. An important future extension of this work would be to directly measure the velocity as a function of vertical position for the different materials to determine the velocity profiles. Measurements of this type are being planned to test the conjectures based on phenomenological flow rule comparisons.

Finally, one must conclude that although the rheology for sand and glass beads seems rather robust and well fit by the Pouliquen/Jenkins form, this is no guarantee that more general materials satisfy this scaling relationship. The copper measurements are puzzling because one

might have expected the nearly spherical copper beads to produce results similar to the spherical glass beads. That the Bagnold form does not seem to apply for copper grains of different shapes and especially for the spherical ones is quite surprising and unexpected. Experiments on other metallic particles would be very helpful in determining the origins of this effect. Finally, a more direct probe of the interior dynamics of granular flows seems essential for determining the bulk flow rheology for general granular media.

This work was funded by the US Department of Energy under Contracts W-7405-ENG & DE-AC52-06NA25396. The authors benefited from discussions with J. Jenkins and I. Aranson. T.B. acknowledges support by the Bolyai Janos research program, and the Hungarian Scientific Research Fund (Contract No. OTKA-F-060157).

- 
- [1] R.A. Bagnold, *Proc. R. Soc. London, Ser. A* 255, 49 (1954).
  - [2] O. Pouliquen, *Phys. of Fluids* 11, No.3, 542 (1999).
  - [3] Y. Forterre and O. Pouliquen, *J. Fluid Mech.* 486, 21 (2003).
  - [4] O. Hungr and N.R. Morgenstern, *Geotechnique* 34, 405 (1984).
  - [5] E. Azzanza, F. Chevoir and P. Moucheron, *J. Fluid Mech.* 400, 199 (1999).
  - [6] C. Ancey, *Phys. Rev. E* 65, 011304 (2001).
  - [7] J. Rajchenbach, *Phys. Rev. Lett.* 90, 144302 (2003).
  - [8] G. Berton, R. Delannay, P. Richard, N. Taberlet and A. Valance, *Phys. Rev. E* 68, 051303 (2003).
  - [9] J. Rajchenbach, *J. Phys.: Condens. Matter* 17, S2731 (2005).
  - [10] G.D.R. Mid, *Eur. Phys. J. E* 14, 341 (2004).
  - [11] H.M. Jaeger, S.R. Nagel and R.P. Behringer, *Rev. Mod. Phys.* 68 1259 (1996).
  - [12] I.S. Aranson and L.S. Tsimring, *Rev. Mod. Phys.* 78 641 (2006).
  - [13] T.S. Komatsu, S. Inagaki, N. Nakagawa and S. Nasuno, *Phys. Rev. Lett.* 86, 1757 (2001).
  - [14] J. Rajchenbach, *Eur. Phys. J. E* 14, 367 (2004).
  - [15] W. Bi, R. Delannay, P. Richard, N. Taberlet and A. Valance, *J. Phys.: Condens. Matter* 17, S2457 (2005).
  - [16] D.V. Kharkhar, A.V. Orpe, P. Andersen and J.M. Ottino, *J. Fluid Mech.*, 441, 255 (2001).
  - [17] N. Taberlet, P. Richard, A. Valance, W. Losert, J.M. Pasini, J.T. Jenkins and R. Delannay, *Phys. Rev. Lett.* 91, 264301 (2003).
  - [18] P. Jop, Y. Forterre and O. Pouliquen, *J. Fluid Mech.*, 541, 167 (2005).
  - [19] T. Borzsonyi, T.C. Halsey and R.E. Ecke, *Phys. Rev. Lett.* 94, 208001 (2005).
  - [20] O. Pouliquen, J. Debur and S.B. Savage, *Nature* 386, 816 (1997).
  - [21] J.T. Jenkins, *Phys. of Fluids* 18, 103307 (2006).
  - [22] L.E. Silbert, D. Ertas, G.S. Grest, T.C. Halsey, D. Levine and S.J. Plimpton, *Phys. Rev. E* 64, 051302 (2001).
  - [23] S. Deboeuf, E. Lajeunesse, O. Dauchot and B. Andreotti, *Phys. Rev. Lett.* 97, 158303 (2006).
  - [24] L.E. Silbert, J.W. Landry and G.S. Grest, *Phys. of Fluids* 15, 1 (2003).
  - [25] T. Borzsonyi and R.E. Ecke, *Phys. Rev. E*, 74, 061301 (2006).
  - [26] S. Douady, A. Manning, P. Hersen, H. Elbelhiti, S. Prost, A. Daerr, B. Kabbachi, *Condmat*, 0412047 (2006).
  - [27] O. Pouliquen and Y. Forterre, *J. Fluid Mech.* 453, 133 (2002).
  - [28] M. van Hecke, private communication.
  - [29] O. Pouliquen and N. Renaut, *J. Phys. II France* 6, 923 (1996).
  - [30] C. Goujon, N. Thomas, and B. Dalboz-Dubrujeaud, *Eur. Phys. J. E* 11, 147 (2003).
  - [31] N. Mitarai and H. Nakanishi, *Phys. Rev. Lett.* 94, 128001 (2005).
  - [32] G. Kuwabara K. Kono, *Jpn. J. Appl. Phys.* 26, 1230 (1987).
  - [33] A.B. Stevens and C.M. Hrenya, *Powd. Tech.* 154, 99 (2005).
  - [34] L.E. Silbert, G.S. Grest, S. Brewster and A.J. Levine, unpublished, (2006).